Proc. of WESIC 2001, University of Twente, The Netherlands, 27-29 June 2001

# MODELLING AND EFFICIENT DYNAMIC SIMULATION OF FLEXIBLE LINK MANIPULATORS

**R.G.K.M. Aarts[†], J.B. Jonker[†] and R.R. Waiboer[†‡]**

[†]University of Twente, Department of Mechanical Engineering,
P.O.Box 217, 7500 AE Enschede, The Netherlands

[‡]Netherlands Institute for Metals Research
P.O. Box 5008, 2600 GA Delft, The Netherlands

Email: R.G.K.M.Aarts@wb.utwente.nl,
J.B.Jonker@wb.utwente.nl,
R.R.Waiboer@wb.utwente.nl

## Abstract

*For accurate simulations of the dynamic behaviour of flexible manipulators the combination of a perturbation method and modal analysis is proposed. First, the vibrational motion is modelled as a first-order perturbation of a nominal rigid link motion. The vibrational motion is then described by a set of linear time-varying equations. Next, applying a modal reduction technique reduces the number of degrees of freedom. The proportional part of the control system is explicitly included in the modal analysis.*
*The applicability and efficiency of the method are demonstrated by simulating the controlled trajectory motion of a spatial flexible three-degree of freedom manipulator with PID control.*

## 1 Introduction

In this paper a perturbation method is proposed for analysing the dynamic behaviour of flexible manipulators, including the effects of the manipulator's control system. It involves a non-linear finite element formulation (Jonker 1990) in which links and joints are considered as specific elements. For an efficient simulation, the non-linear equations of motion are linearised in the so-called perturbation method. The dimension of the linearised system is reduced with a modal reduction technique that we refer to as the Adaptive Modal Integration (AMI) method.

The non-linear finite element formulation and the proposed solution method are implemented in the program SPACAR (Jonker & Meijaard 1990). An interface to MATLAB is available and simulations are carried out using SIMULINK's graphical user interface. A spatial flexible three-degree of freedom manipulator (Fig. 1) with PID

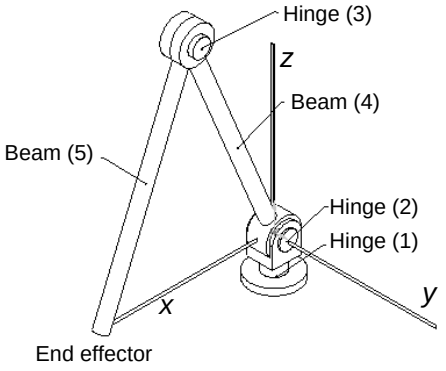


Figure 1: Spatial two-link manipulator.

control is analysed to illustrate the solution method. Results from a non-linear simulation are compared with the perturbation method with and without modal reduction (Sect. 3). In earlier papers we discussed the applicability of the non-linear simulations (Jonker & Meijaard 1990, Jonker & Aarts 1998) and the perturbation method (Jonker & Aarts 2001). The modal analysis and reduction have been introduced in (Aarts & Jonker 2000). In the next section only a course outline will be given.

# 2 Equations of motion

In the non-linear finite element formulation (Jonker 1990) links and joints are considered as specific elements. The governing equations of motion are derived in two sets of co-ordinates. The first set represents the generalised co-ordinates of the manipulator with rigid links used to express control forces and torques, i.e. the actuator joint co-ordinates denoted $\underline{e}^m$. The second set consists of the deformation co-ordinates $\underline{\varepsilon}^m$ that characterise flexible deformations of the links. The non-linear equations of motion can be written as

$$\bar{M}(\underline{q})\ddot{\underline{q}} + C(\underline{q},\dot{\underline{q}})\dot{\underline{q}} + \underline{g}(\underline{q}) = -\begin{bmatrix} \underline{\sigma}^{em} \\ \underline{\sigma}^{\varepsilon m} \end{bmatrix}, \tag{1}$$

where the vector of generalised co-ordinates is

$$\underline{q} = \begin{bmatrix} \underline{e}^m \\ \underline{\varepsilon}^m \end{bmatrix}. \tag{2}$$

The reduced mass matrix $\bar{M}$ in Eq. (1) can be written as

$$\bar{M} = \begin{bmatrix} \bar{M}^{ee} & \bar{M}^{e\varepsilon} \\ \bar{M}^{\varepsilon e} & \bar{M}^{\varepsilon\varepsilon} \end{bmatrix}, \tag{3}$$

to explicitly indicate the $\underline{e}^m$ and $\underline{\varepsilon}^m$ parts of the matrix. The second term $C(\underline{q},\dot{\underline{q}})\dot{\underline{q}}$ represents the Coriolis and centrifugal forces and $\underline{g}(\underline{q})$ is the vector of external nodal forces, including gravitational forces. The driving forces and torques, represented by the vector $\underline{\sigma}^{em}$, are applied only at the actuator joints. If actuator dynamics are not considered then there is a simple linear relation between the vector of control inputs $\underline{u}$ and the vector $\underline{\sigma}^{em}$

$$\underline{\sigma}^{em} = -\underline{u}. \tag{4}$$

The stress resultant vector of flexible elements is characterised by Hooke's law defined by $\underline{\sigma}^{\varepsilon} = K^{\varepsilon\varepsilon}\underline{\varepsilon}$, where $K^{\varepsilon\varepsilon}$ is a symmetric matrix containing the elastic constants.

As the direct solution of the non-linear equations of motion is rather time consuming, a two-step perturbation approach has been developed. In this approach the vibrational motion of the manipulator is modelled as a first-order perturbation of the nominal rigid link motion, where the vibrations are the elastic motions and the perturbations in the rigid link motion. This is expressed by writing the generalised co-ordinates as

$$\underline{q} = \underline{q}_0 + \delta\underline{q}, \tag{5}$$

where the subscript $0$ is used for the nominal trajectory and the prefix $\delta$ denotes a perturbation. In the first step the nominal rigid link motion is described by the rigidified manipulator model. That is a non-linear model in which all flexible deformation co-ordinates are prescribed zero, i.e. $\underline{\varepsilon}^m \equiv \underline{0}$. In a dynamic analysis the equations of motion are symbolically linearised and evaluated numerically in a number of points of the nominal trajectory. In addition, generalised stress resultants of the rigidified links $\underline{\sigma}_0^{\varepsilon m}$ are computed. The input force vector is equal to $\underline{u}_0$ which represents the vector of nominal input forces and torques necessary to move the rigid link manipulator along the nominal (desired) trajectory. During the second step the vibrational motion is described by a set of linear time-varying equations using the linearised description. The generalised stress resultants are applied as internal excitation forces. The actuator input is now $\delta\underline{u}$ which is the control input vector synthesised at the stage of perturbed dynamics. It is assumed that the control input vector $\delta\underline{u}$ can be written as

$$\delta\underline{u} = -K_p\delta\underline{e}^m + \delta\underline{u}_{\mathrm{d}}, \tag{6}$$

where the matrix $K_p$ represents the proportional action of the controller and the remaining *dynamic* action is described by $\delta\underline{u}_{\mathrm{d}}$. The vibrational motion is then described by a set of inhomogeneous linear time-varying equations of the form

$$\bar{M}_0\delta\ddot{\underline{q}} + C_0\delta\dot{\underline{q}} + \bar{K}_0\delta\underline{q} = \underline{\sigma}_0, \tag{7}$$

where the right-hand side vector is

$$\underline{\sigma}_0 = \begin{bmatrix} \delta\underline{u}_{\mathrm{d}} \\ \underline{\sigma}_0^{\varepsilon m} \end{bmatrix}. \tag{8}$$

The system mass matrix $\bar{M}_0$ accounts for the inertia properties as in Eq. (1), $C_0$ is the velocity sensitivity matrix, and the combined stiffness matrix $\bar{K}_0$ is defined as

$$\bar{K}_0 = \begin{bmatrix} 0 & 0 \\ 0 & K_0^{\varepsilon\varepsilon} \end{bmatrix} + G_0 + N_0 + \begin{bmatrix} K_p & 0 \\ 0 & 0 \end{bmatrix}, \tag{9}$$

to include the proportional control matrix $K_p$ in addition to the structural stiffness matrix $K_0^{\varepsilon\varepsilon}$, the geometric stiffening matrix $G_0$ and the dynamic stiffening matrix $N_0$. $\bar{M}_0$, $K_0$ and $G_0$ are symmetric matrices, but $C_0$ and $N_0$ need not. These matrices are calculated using an analytical linearisation method (Meijaard 1991). The matrix coefficients depend on the nominal position, velocity and acceleration of the manipulator and consequently they are time-varying.

To reduce the dimension of the linearised system, a modal reduction technique is proposed. Analogously to e.g. (Craig 1981) the key step in the modal analysis is the introduction of a co-ordinate transformation

$$\delta\underline{q} = \Phi\underline{\eta}, \tag{10}$$

where the $n$ elements of the vector $\underline{\eta}$ are the so-called principal co-ordinates $\eta_i$. The columns of the modal matrix $\Phi$ are the natural modes $\underline{\phi}_i$. These modes and the natural frequencies $\omega_i$ are found by solving the eigenvalue problem with the mass and stiffness matrices $\bar{M}_0$ and $\bar{K}_0$ as in (Aarts & Jonker 2000). According to Eq. (9) the mode shape functions are then determined by taking into account the proportional feedback gains associated with the rigid link motion. Unfortunately, the dynamic stiffening term $N_0$ in the stiffness matrix is in general not symmetric. Hence the system described by $\bar{M}_0$ and $\bar{K}_0$ is circulatory and the solution of the eigenvalue problem may lead to natural frequencies and modes with imaginary parts. To avoid these solutions we consider the eigenvalue problem

$$(\bar{K}_0^{\mathrm{S}} - \omega_i^2 \bar{M}_0)\underline{\phi}_i = 0 \qquad (i = 1, 2, ..., n), \tag{11}$$

in which a symmetric stiffness matrix is used

$$\bar{K}_0^{\mathrm{S}} = \frac{1}{2}(\bar{K}_0 + \bar{K}_0^{\mathrm{T}}). \tag{12}$$

This symmetric matrix $\bar{K}_0^{\mathrm{S}}$ is only used to compute the modal matrix $\Phi$. The linearised equations of motion are solved with the original $\bar{K}_0$. As the mass and stiffness matrices are time-varying, the natural frequencies and the modal matrix are functions of the time. The time-varying nature of the mode shape functions has to be taken into account in the modal analysis.

Finally the reduction of the dimension of the system is accomplished by considering only $\hat{n} < n$ (low frequency) modes. Unfortunately, in many practical cases this straightforward reduction is not accurate, unless many modes are taken into account. Improved convergence properties are found using the mode-acceleration concept in which the pseudo-static response of the remaining $n$-$\hat{n}$ (high frequency) principal co-ordinates is taken into account.

The modal reduction technique outlined above will be referred to as the Adaptive Modal Integration (AMI) method. It has been integrated with our implementation of the finite element program SPACAR (Jonker & Meijaard 1990, Jonker & Aarts 1998, Jonker & Aarts 2001), with which the nominal trajectories are computed and the linearisation is carried out at $N$ discrete time steps $t = t_i$ ($i = 0, 1, 2, ..., N$). To solve the linearised equations a so-called LTV block has been developed for use in a SIMULINK model (SIMULINK 1999). Within the SIMULINK framework this LTV block represents a linear time-varying state space system (Jonker & Aarts 1998, Jonker & Aarts 2001).

# 3 Simulation example

## 3.1 System properties

To investigate the applicability of the perturbation method the controlled motion of a spatial two-link flexible manipulator in a gravitational field is studied. Figure 1 illustrates the finite element representation of this manipulator. The revolute joints of the manipulator are modelled by the hinge elements (1), (2) and (3). The rotational axes of the hinge elements (2) and (3) are parallel, thus providing the in-plane motion of the manipulator. The vertical axis of hinge (1) coincides with the $z$ axis. The hinges are driven by internal actuators, which are modelled as pure torque sources without dynamics. The two links of the manipulator, modelled by beam elements (4) and (5), are

| Beam number | 4 | 5 |
|---|---|---|
| Length $l$ (m) | 0.7 | 0.7 |
| Bending stiffness $EI/l^3$ (N/m) | 48300 | 24460 |
| Torsion stiffness $GI_p/l^3$ (N/m) | 41580 | $\infty$ |
| Mass per unit length $m$ (kg/m) | 4 | 2 |

Table 1: Kinematic and dynamic link parameters.

respectively referred to as upper arm and forearm. Both arms have uniform cross sections and are assumed to be flexible. The longitudinal deformations in both arms and the torsional deformation in the forearm are suppressed. Table 1 lists the relevant kinematic and dynamic properties of the links. A small internal damping is assumed which leads to relative damping equal to 0.002 for the lowest natural mode. The masses of the bearing assembly at the elbow hinge (3) and of the end effector are modelled by point masses of 10 kg and 30 kg, respectively. The gravity loads, including the loads due to the distributed mass of the links, are taken into account by applying the corresponding external forces in the negative $z$ direction. The total model has nine flexible degrees of freedom in addition to the actuator joint co-ordinates $e_1$, $e_2$ and $e_3$ representing the relative rotations of the actuators.

## 3.2 Controlled trajectory motion

The manipulation task implies transferring the manipulator tip along a straight line with a smooth velocity profile, see Fig. 2(a) and (b). The acceleration and deceleration in the velocity profile is composed of squared sines. The torques are governed by a control algorithm consisting of an open-loop and a closed-loop component. Solving the inverse kinematic and dynamic problem of the rigidified model of the manipulator yields the necessary nominal actuator moments $\underline{u}_0$ of Fig. 2(c) which are applied as open-loop feedforward torques. In addition a MIMO PID feedback controller is used in which the position sensors are collocated with the actuators. The control law is given

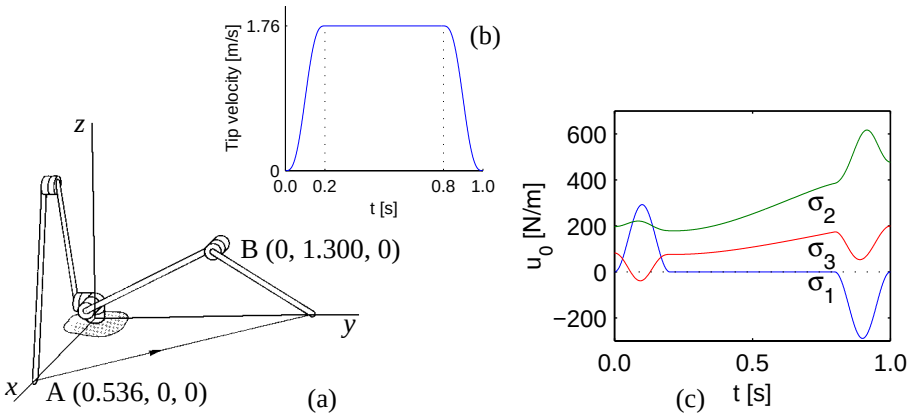


Figure 2: (a) Motion trajectory and (b) velocity profile of the manipulator tip.
(c) Nominal torques $\underline{u}_0$ for the three actuators.

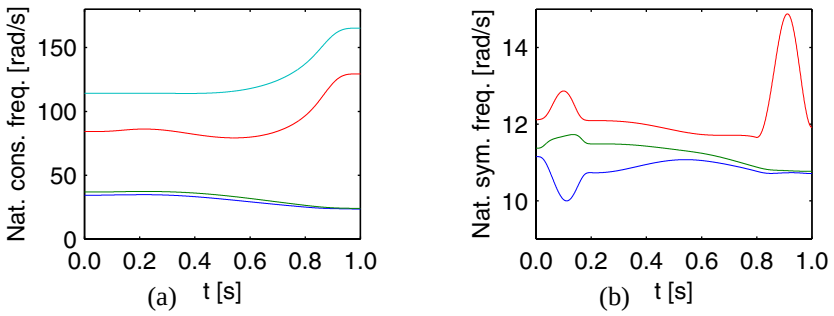


Figure 3: (a) Four lowest natural frequencies $\omega_{c,i}$ for a constraint manipulator, Eq. (16). (b) Three lowest closed-loop natural frequencies $\omega_i$ during the controlled trajectory motion of the manipulator computed with a symmetric $\bar{K}_0^{\mathrm{S}}$ as in Eq. (11).

by

$$\delta \underline{u} = -\bar{M}_0^{ee}\, H(s)\, \delta \underline{e}^m. \tag{13}$$

The coupling between the actuators is represented by the time dependent mass matrix $\bar{M}_0^{ee}$. The controller $H(s)$ has only three diagonal components, each of which is a SISO PID controller

$$H_i(s) = k_{p,i} \frac{\tau_{I,i} s + 1}{\tau_{I,i} s} \frac{\tau_{D,i} s + 1}{\alpha_i \tau_{D,i} s + 1} \qquad (i = 1, 2, 3), \tag{14}$$

where $k_{p,i}$ is the proportional gain and $\alpha_i$, $\tau_{D,i}$ and $\tau_{I,i}$ determine the zero and pole positions of the controller. For each controller these parameters are taken

$$\begin{aligned} k_{p,i} &= \omega_{b,i}^2, \\ \tau_{I,i} &= 6/\omega_{b,i}, \\ \tau_{D,i} &= 1.5/\omega_{b,i}, \\ \alpha_i &= 0.1, \end{aligned} \tag{15}$$

in which $\omega_{b,i}$ are the desired servo loop frequencies. In principal each loop can be tuned separately, where $\omega_{b,i}$ should be chosen sufficiently low with respect to the natural frequencies of the system to avoid instabilities.

The inertia properties depend on the configuration, so the mass matrix $\bar{M}_0^{ee}$ in Eq. (13) changes during the simulation. For the specified initial and final configuration some of the terms differ by a factor of 6. Hence the mass matrix $\bar{M}_0^{ee}$ has to be updated during the motion.

Analogous to the approach of (Book et al. 1975) the servo loop frequencies $\omega_{b,i}$ are chosen with respect to the lowest *constraint* natural frequencies $\omega_{c,i}$ of the system. In the constraint system all actuator joint co-ordinates $\underline{e}^m$ are prescribed and thus $\delta \underline{e}^m = 0$. The associated frequency equation is then given by

$$\det(-\omega_{c,i}^2 \bar{M}_0^{\varepsilon\varepsilon} + \bar{K}_0^{\varepsilon\varepsilon}) = 0. \tag{16}$$

For the considered motion the lowest frequency changes only gradually from 34 rad/s to 24 rad/s, see Fig. 3(a). With fixed setting $\omega_b = 12$ rad/s for all $\omega_{b,i}$ a stable controller is expected. The proportional part of the control law is then

$$K_p = \omega_b^2 M_0^{ee}. \tag{17}$$

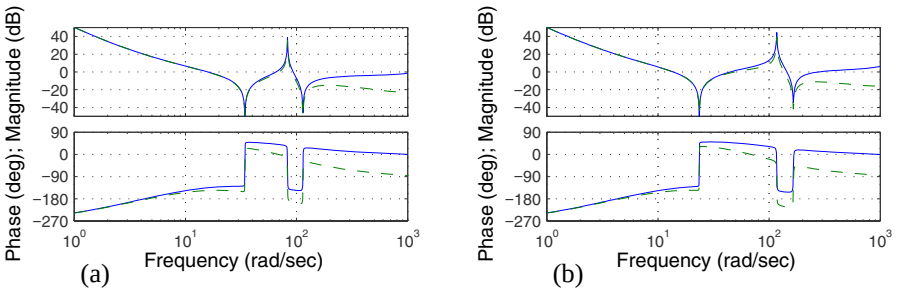


Figure 4: Bode plots of the open loop SISO system for actuator 1. The solid lines are with the PID controller of Eq. (14); the dashed lines are with an additional pole in $-1/\alpha_i\tau_{D,i}$. Graph (a) is for the initial configuration and (b) for the final configuration.

Using this value the natural frequencies of Eq. (11) have been calculated and the lowest three closed-loop natural frequencies are shown in Fig. 3(b). The increase of the third natural frequency near $t = 0.9$ s is caused by dynamic stiffening. It should be noted that these natural frequencies are computed with the symmetric stiffness matrix $\bar{K}_0^{\mathrm{S}}$. In case the true stiffness matrix $\bar{K}_0$ is used, complex natural frequencies are found near $t = 0.1$ s and $0.6$ s.

The linearised equations of motion also provide a powerful method to analyse the designed controller. Main idea of using the mass matrix $\bar{M}_0^{ee}$ in the controller Eq. (13) is to decouple the actuators into three SISO systems. This will match perfectly for a rigid manipulator of which the parameters are known exactly. However, for flexible links coupling terms will remain between actuators. By inspection of the open-loop system of controller and linearised system it was observed that actuator 1 behaves like a SISO system and that there is a coupling between actuators 2 and 3.

The controller design is not further optimised in this paper, but its performance is partly illustrated in Fig. 4 which shows the Bode plots for the SISO system of actuator 1. Only the initial and final configurations are presented, but obviously the stability along the whole trajectory can be studied. The PID controller of Eq. (14) does not include roll-off, so the magnitude of the vibrational mode near 100 rad/s is quite large. A positive phase margin remains, so this controller does not lead to unstable oscillations in the frequency range that is shown. A (too simple) attempt to add roll-off with an additional controller pole in $-1/\alpha_i\tau_{D,i}$ will *not* work as the Bode plots clearly show that for this system the vibrational mode becomes unstable, especially in the final configuration. Simulations as discussed in the next section can confirm this behaviour.

## 3.3 Simulation results

The simulations have been carried out using SIMULINK's `ode45` variable time step Runge-Kutta solver with the *relative tolerance* set to $10^{-4}$ (SIMULINK 1999). Results from three methods are compared: the non-linear finite element method, the perturbation method with the number of linearisation points $N = 1500$ and the AMI method with $\hat{n} = 4$ (the number of modes). In a previous paper (Jonker & Aarts 2001) we showed that using less linearisation points leads to larger differences between the non-linear simulation and the perturbation method for this manipulator motion with a PD controller. Increasing $N$ further does not improve the accuracy.

Figure 5 shows the deviation from the nominal trajectory for the actuator angles

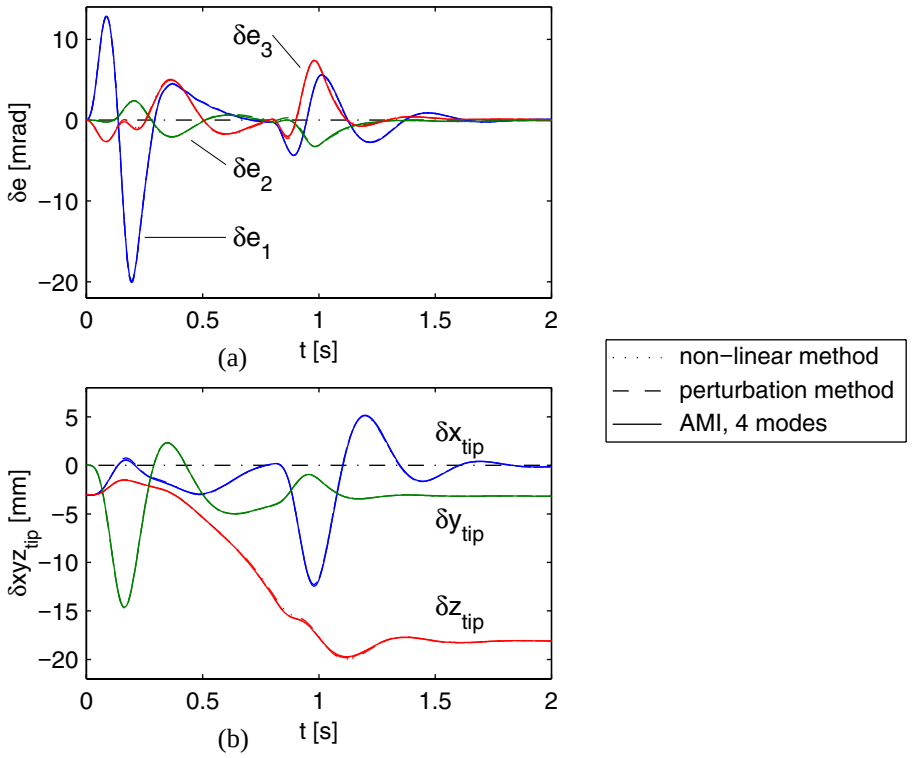


Figure 5: Deviation from the nominal trajectory according to three simulation methods: (a) actuator rotations and (b) tip co-ordinates.

and the manipulator tip position according to these three methods. In all simulations the manipulator is at rest at $t = 0$ s. The integral action of the PID controllers results in zero errors for the actuator angles. The initial deformations of the links are computed from the steady solution which is found by splitting the steady part of Eq. (7) into

$$\begin{aligned} \bar{K}_0^{ee}\delta\underline{e}^m + \bar{K}_0^{e\varepsilon}\underline{\varepsilon}^m &= \delta\underline{u}_\mathrm{d}, \\ \bar{K}_0^{\varepsilon e}\delta\underline{e}^m + \bar{K}_0^{\varepsilon\varepsilon}\underline{\varepsilon}^m &= \underline{\sigma}_0^{\varepsilon m}. \end{aligned} \tag{18}$$

As $\delta\underline{e}^m = 0$, the link deformations $\underline{\varepsilon}^m$ can be solved from the second set of equations. The initial integral controller action $\delta\underline{u}_\mathrm{d}$ follows then immediately from the first set of equations. The deviations from the nominal position are in the $xz$-plane, which is clearly expressed by the non-zero $\delta x_\mathrm{tip}$ and $\delta z_\mathrm{tip}$ at $t = 0$ s in Fig. 5(b). For $0\text{ s} < t < 1$ s the manipulator moves along the trajectory. The effects of acceleration and deceleration can be seen in Fig. 5. Clearly, all simulations show that the proposed controller is stable and the manipulator is practically at rest for $t > 1.7$ s. The deviations from the nominal position are now in the $yz$-plane, which results in non-zero $\delta y_\mathrm{tip}$ and $\delta z_\mathrm{tip}$. Obviously, the deviation in the $z$ direction is larger than at $t = 0$ s as the distance of the tip of the manipulator to the origin is larger.

Some differences are found between the simulations in Fig. 5. The $z$ position for $t \approx 0.85$ s is slightly lower according to the perturbation method than the non-linear result. This error of approximately 0.26 mm is hardly visible on the scale of the graph. It illustrates the accuracy that can be obtained with the linearised model. Subsequent

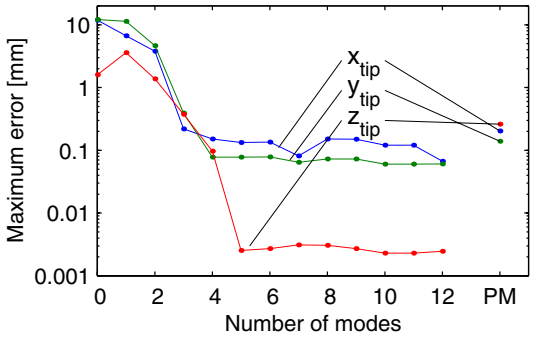


| CPU time | |
|---|---|
| AMI 3 modes | 70 s |
| AMI 4 modes | 100 s |
| AMI 5 modes | 410 s |
| Perturbation method | 265 s |
| Non-linear simulation | 1100 s |

Figure 6: Maximum errors in the co-ordinates of the tip position as functions of the number of modes. The error is computed by comparing the AMI method with the perturbation method. For comparison the dots indicated with "PM" show the maximum difference between the perturbation method and the non-linear simulation.
The table on the right illustrates the amount of CPU time for some of the simulations.

modal reduction to 4 modes does not affect the accuracy as the results from the AMI method can not be distinguished from the perturbation method in Fig. 5. The maximum deviation from the perturbation method is found for $\delta x_{\,\mathrm{tip}}$ near $t = 1.04$ s and is about 0.15 mm.

The error introduced by the modal reduction is illustrated in more detail in Fig. 6 where for each tip co-ordinate the maximum error along the trajectory is plotted as a function of the number of modes. Obviously, by taking into account only 3 modes the error is already comparable to the error that was introduced by the linearisation. Simulating with more modes only leads to the inclusion of modes with higher natural frequencies which slow down the simulations without improving the accuracy. This is demonstrated clearly in the table next to the graph which shows the required CPU time for some simulations. A simulation using the AMI method with 3 or 4 modes is efficient as the $5^{\mathrm{th}}$ mode apparently leads to a significant increase in the required CPU time, but hardly improves the accuracy.

# 4 Conclusions

The presented perturbation method allows an efficient numerical simulation of the controlled trajectory motion of a flexible manipulator as well as a straightforward vibration control formulation. A further reduction of the simulation time was obtained by applying a modal reduction technique, which we refer to as the Adaptive Modal Integration (AMI) method. For the spatial flexible two-link manipulator, results of both the perturbation method and the AMI method agree well with the results obtained from a full non-linear analysis. In the AMI method only three (modified rigid link) of four degrees of freedom are needed to reach a satisfying accuracy. Crucial elements in the AMI method are the availability of accurate linearised equations and a careful modal analysis in which the time-varying nature of the mode shape functions and the proportional feedback gains are taken into account.

## Acknowledgements

The authors acknowledge the work carried out by H. Super on the implementation and simulations of the perturbation method with modal analysis. Part of this research was carried out under project number MC8.00073 in the framework of the Strategic Research programme of the Netherlands Institute for Metals Research in the Netherlands (http://www.nimr.nl/).

## References

Aarts, R. & Jonker, J. (2000). Dynamic simulation of flexible link manipulators using adaptive modal integration, *in* J. Ambrósio & M. Kleiber (eds), *NATO Advanced Research Workshop on Computational Aspects of Nonlinear Structural Systems with Large Rigid Body Motion*, Pultusk, Poland, pp. 165–180.

Book, W., Maizza-Neto, O. & Withney, D. (1975). Feedback control of two beam, two joint systems with distributed flexibility, *Journal of Dynamic Systems, Measurement and Control* **97**: 424–431.

Craig, R. R. (1981). *Structural Dynamics: An Introduction to Computer Methods*, John Wiley and Sons, New York.

Jonker, J. (1990). A finite element dynamic analysis of flexible manipulators, *The international Journal of Robotics Research* **9**(4): 59–74.

Jonker, J. & Aarts, R. (1998). Modelling of flexible mechanisms and manipulators for control purposes, *Proceedings of the Fourth International Conference on Motion and Vibration Control, MoViC*, Vol. 1, Institute of Robotics, ETH-Zurich, pp. 291–297.

Jonker, J. & Aarts, R. (2001). A perturbation method for dynamic analysis and simulation of flexible manipulators, accepted for publication in *Multibody Systems Dynamics* .

Jonker, J. & Meijaard, J. (1990). Spacar-computer program for dynamic analysis of flexible spatial mechanisms and manipulators, *in* W. Schiehlen (ed.), *Multibody Systems Handbook*, Springer-Verlag, Berlin, pp. 123–143.

Meijaard, J. (1991). Direct determination of periodic solutions of the dynamical equations of flexible mechanisms and manipulators, *International Journal of Numerical Methods in Engineering* **32**: 1691–1710.

SIMULINK(1999). *Dynamic System Simulation for* MATLAB, *Using* SIMULINK *version 3*, The MathWorks Inc., Natick (MA).